Molecular Cell, Volume *72*

Supplemental Information

The Histone Chaperone FACT Coordinates

H2A.X-Dependent Signaling and Repair of DNA Damage

Sandra Piquet, Florent Le Parc, Siau-Kun Bai, Odile Chevallier, Salomé Adam, and Sophie E. Polo

Figure S1

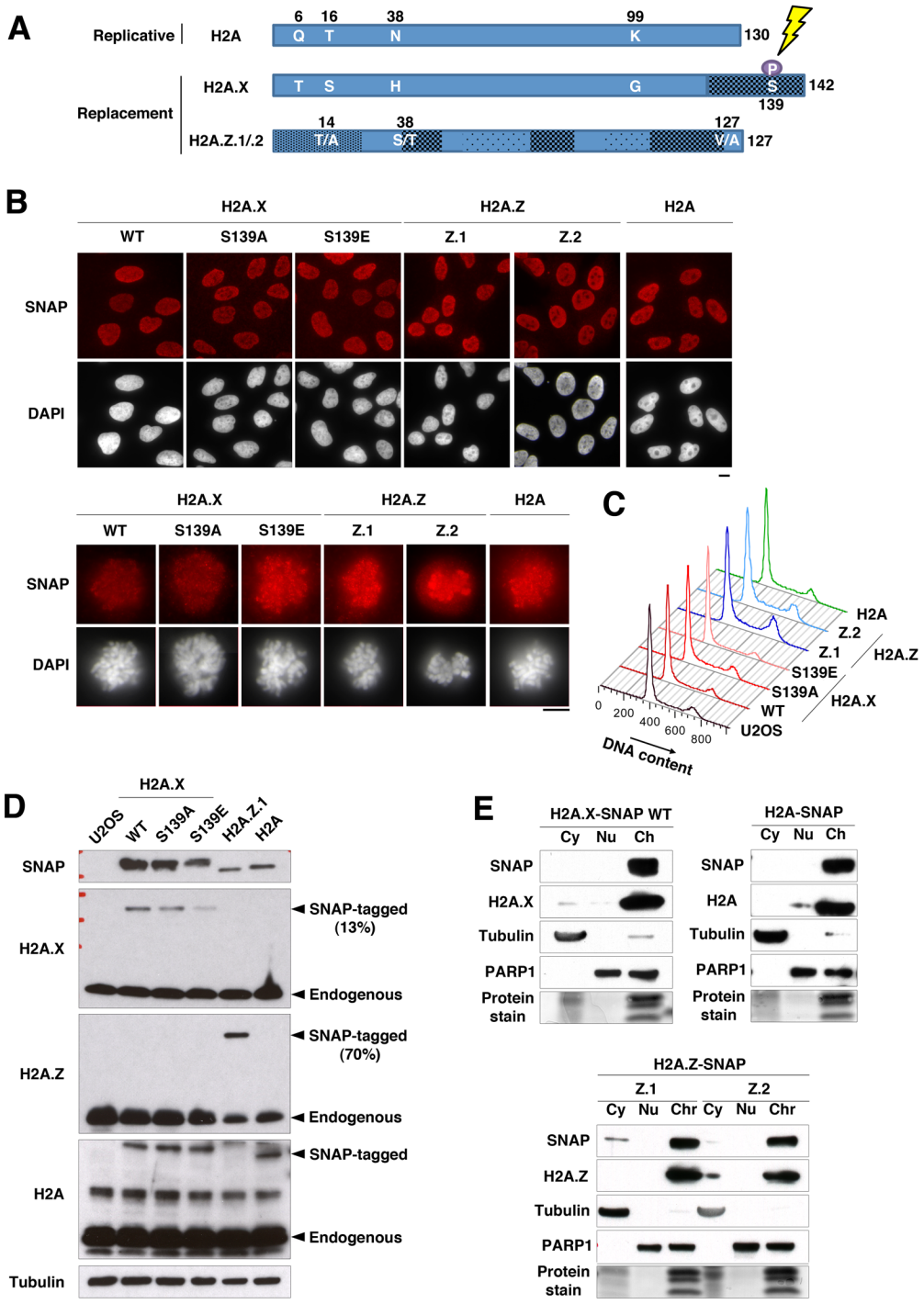
A
Replicative
H2A
6 16 38 99
Q T N K
130
Replacement
H2A.X
T S H G S
P
142
139
H2A.Z.1/.2
14 38 127
T/A S/T V/A
127
B
H2A.X
H2A.Z
H2A
WT
S139A
S139E
Z.1
Z.2
SNAP
DAPI
C
H2A
Z.2
Z.1
H2A.Z
S139E
S139A
WT
H2A.X
U2OS
0
200
400
600
800
DNA content
D
H2A.X
U2OS
WT
S139A
S139E
H2A.Z.1
H2A
SNAP
H2A.X
SNAP-tagged (13%)
Endogenous
H2A.Z
SNAP-tagged (70%)
Endogenous
H2A
SNAP-tagged
Endogenous
Tubulin
E
H2A.X-SNAP WT
Cy Nu Ch
SNAP
H2A.X
Tubulin
PARP1
Protein stain
H2A-SNAP
Cy Nu Ch
SNAP
H2A
Tubulin
PARP1
Protein stain
H2A.Z-SNAP
Z.1
Z.2
Cy Nu Chr Cy Nu Chr
SNAP
H2A.Z
Tubulin
PARP1
Protein stain

Figure S1: Characterization of H2A variant-SNAP cell lines. Related to Figures 1 and 2.

(A) Schematic representation of the H2A variants studied in this work. Residues that differ between variants are indicated in white and more divergent portions of the proteins are shaded in black. The phosphorylatable Ser139 on H2A.X is highlighted.

(B) Comparable expression levels and nuclear localization of SNAP-tagged H2A variants analyzed by immunofluorescence against SNAP in U2OS cells stably expressing the indicated SNAP-tagged H2A variants. Images for H2A.Z.2-SNAP cells were acquired separately but showed comparable expression levels of SNAP-tagged histones compared to H2A.Z.1-SNAP cells. For H2A.X variants, WT: wild-type; S139A: Ser139 mutated to Ala, phospho-deficient; S139E: Ser139 mutated to Glu, phospho-mimetic. The upper panel shows representative fields of cells and the bottom panel shows that all SNAP-tagged H2A variants decorate mitotic chromosomes, indicative of their proper incorporation into chromatin. Scale bars, 10 μm

(C) Cell cycle profiles of the indicated cell lines analyzed by flow cytometry (U2OS: parental cell line). The expression of SNAP-tagged H2A variants does not result in overt cell cycle perturbations.

(D) Western-blot analysis of the expression of SNAP-tagged histones on total extracts from the different U2OS cell lines compared to parental U2OS, using the indicated antibodies. The percentages indicate the relative amount of SNAP-tagged protein (H2A.X WT or H2A.Z) relative to the endogenous form. Quantification was not possible for H2A because the antibody cross-reacts with H2A.X.

(E) Western-blot analysis of cytosolic (Cy), nuclear (Nu) and chromatin (Ch) fractions prepared from the indicated cell lines. Like endogenous histones, SNAP-tagged histones (SNAP) are mostly chromatin-bound. Tubulin and PARP1 immunodetection and histone proteins revealed by protein stain are used as controls for the efficiency of the fractionation.

Figure S2

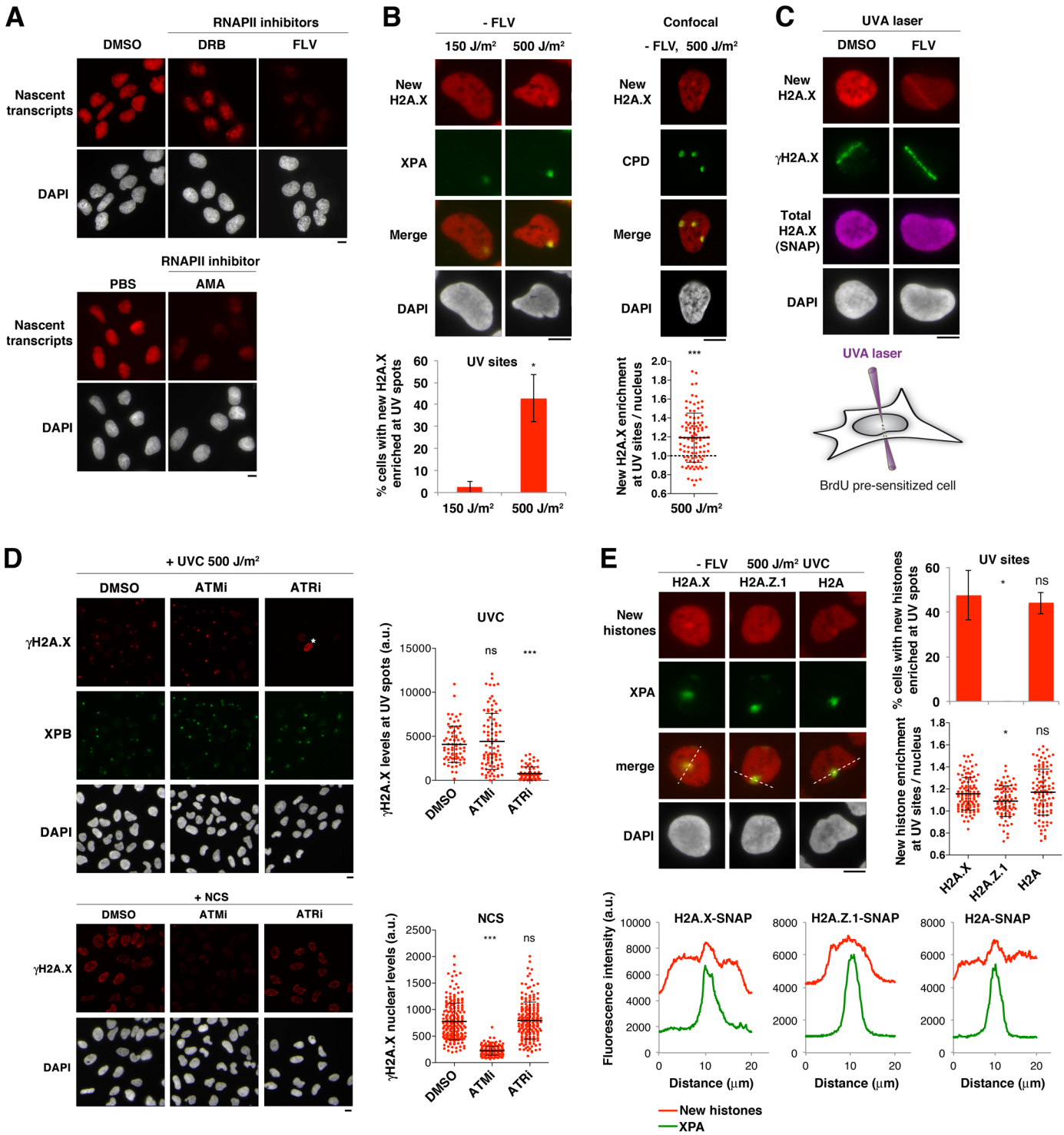
A
RNAPII inhibitors
DMSO
DRB
FLV
Nascent transcripts
DAPI
RNAPII inhibitor
PBS
AMA
Nascent transcripts
DAPI
B
- FLV
150 J/m²
500 J/m²
New H2A.X
XPA
Merge
DAPI
% cells with new H2A.X enriched at UV spots
UV sites
150 J/m²
500 J/m²
Confocal
- FLV, 500 J/m²
New H2A.X
CPD
Merge
DAPI
New H2A.X enrichment at UV sites / nucleus
500 J/m²
C
UVA laser
DMSO
FLV
New H2A.X
γH2A.X
Total H2A.X (SNAP)
DAPI
UVA laser
BrdU pre-sensitized cell
D
+ UVC 500 J/m²
DMSO
ATMi
ATRi
γH2A.X
XPB
DAPI
+ NCS
DMSO
ATMi
ATRi
γH2A.X
DAPI
UVC
γH2A.X levels at UV spots (a.u.)
DMSO
ATMi
ATRi
NCS
γH2A.X nuclear levels (a.u.)
DMSO
ATMi
ATRi
E
- FLV
500 J/m² UVC
H2A.X
H2A.Z.1
H2A
New histones
XPA
merge
DAPI
UV sites
% cells with new histones enriched at UV spots
New histone enrichment at UV sites / nucleus
H2A.X
H2A.Z.1
H2A
Fluorescence intensity (a.u.)
H2A.X-SNAP
H2A.Z.1-SNAP
H2A-SNAP
Distance (μm)
New histones
XPA

Figure S2: *De novo* deposition of H2A variants at repair sites. Related to Figures 1 and 2.

(A) Efficiency of transcription inhibition in U2OS H2A.X-SNAP cells treated with the indicated RNAPII inhibitors (DRB; FLV, flavopriridol; AMA, α-amanitin; DMSO and PBS: vehicles) measured by Ethynyl-Uridine incorporation into nascent transcripts.

(B) New H2A.X accumulation at sites of UVC damage (XPA, CPD) revealed 2 h after irradiation in the absence of flavopiridol (- FLV) upon high UVC dose (500 J/m^2). Right, confocal images. Percentages of cells accumulating new H2A.X at UV sites are shown on the graph and the enrichment of new H2A.X at UV sites relative to the whole nucleus is presented on the scatter plot (bar: mean; error bars: SD from 99 UV spots; the significance of H2A.X enrichment at UV sites is indicated, compared to a theoretical mean of 1, dotted line).

(C) New H2A.X accumulation at sites of UVA laser damage marked by γH2A.X analyzed 2 h after irradiation in U2OS cells stably expressing H2A.X-SNAP.

(**D**) We assessed whether UVC irradiation was triggering a DSB response at the time of new H2A.X deposition by examining the dependency of H2A.X phosphorylation on ATM (ataxia telangiectasia mutated) and ATR kinases using specific inhibitors. ATM is known to phosphorylate H2A.X in response to DSBs. We observed that H2A.X phosphorylation upon local UVC irradiation was strictly ATR- and not ATM-dependent, as opposed to H2A.X phosphorylation following treatment with the DSB-inducing drug neocarzinostatin (NCS), which was strictly ATM-dependent: γH2A.X levels at sites of UVC irradiation (top) and upon cell exposure to the DSB-inducing agent neocarzinostatin (NCS) analyzed in U2OS cells treated with the indicated inhibitors (ATMi, ATRi; DMSO, vehicle). UVC-irradiated cells with pan-nuclear γH2A.X upon ATR inhibition (replicative stress, asterisk) were excluded from the analysis. The intensity of γH2A.X signal at UVC damage sites (delineated by XPB staining) and in the nucleus of NCS-treated cells is shown on the scatter plots (bars: mean; error bars: SD from at least 67 UVC spots and 195 NCS-treated cells). Similar results were obtained in three independent experiments and data from one representative experiment are shown.

(E) *De novo* accumulation of the indicated H2A variants at sites of UVC damage (XPA) revealed 2 h after irradiation in the absence of flavopiridol (- FLV) upon high UVC dose (500 J/m^2). Fluorescence intensity profiles along the dotted lines are shown on the graphs. Percentages of cells accumulating new H2A variants at UV sites are shown on the bar chart and the enrichment of new H2A variants at UV sites relative to the whole nucleus is presented on the scatter plot (bar: mean; error bars: SD from at least 85 UV spots).

Error bars on the bar charts represent SD from two independent experiments. Scale bars, 10 μm.

Figure S3

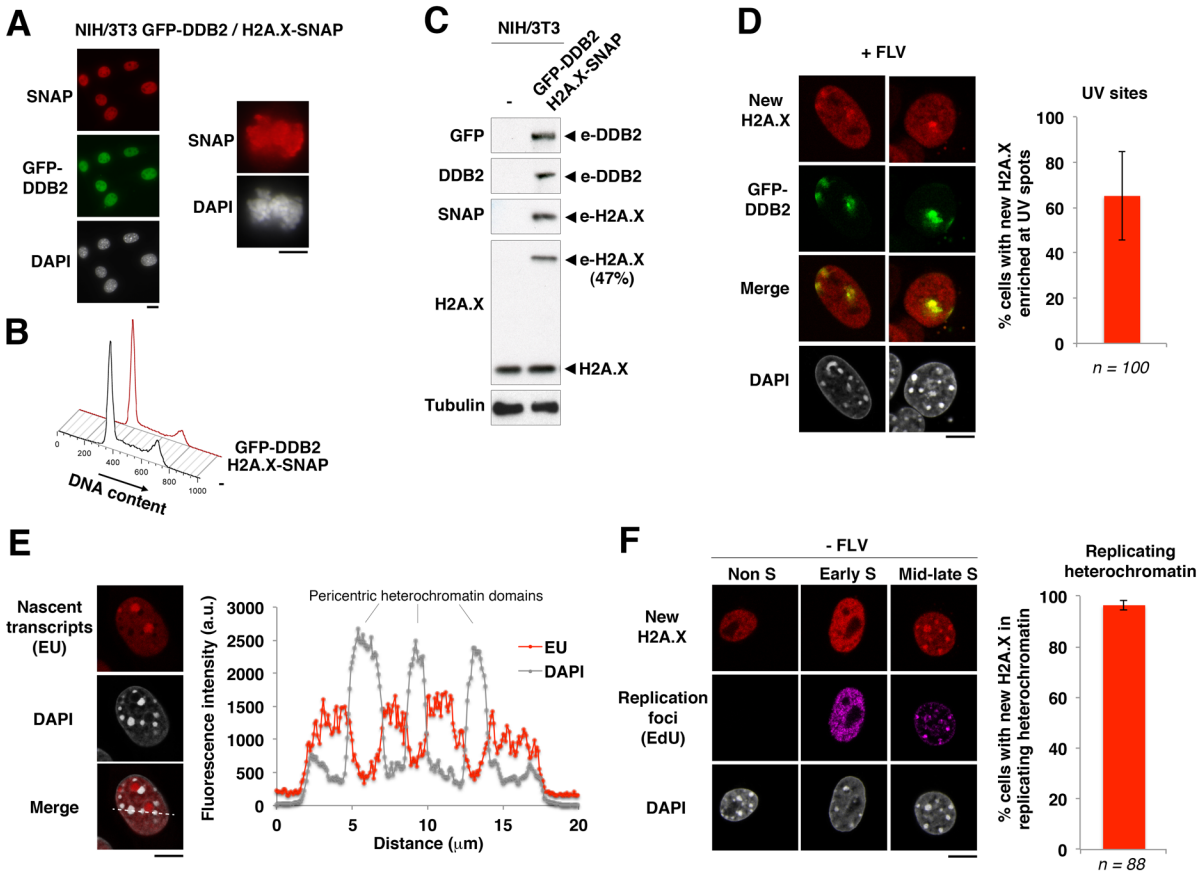
A
NIH/3T3 GFP-DDB2 / H2A.X-SNAP
SNAP
GFP-DDB2
DAPI
SNAP
DAPI
B
GFP-DDB2
H2A.X-SNAP
-
DNA content
C
NIH/3T3
-
GFP-DDB2
H2A.X-SNAP
GFP
DDB2
SNAP
H2A.X
Tubulin
e-DDB2
e-DDB2
e-H2A.X
e-H2A.X
(47%)
H2A.X
D
+ FLV
New H2A.X
GFP-DDB2
Merge
DAPI
UV sites
% cells with new H2A.X enriched at UV spots
n = 100
E
Nascent transcripts (EU)
DAPI
Merge
Pericentric heterochromatin domains
Fluorescence intensity (a.u.)
EU
DAPI
Distance (μm)
F
- FLV
Non S
Early S
Mid-late S
New H2A.X
Replication foci (EdU)
DAPI
Replicating heterochromatin
% cells with new H2A.X in replicating heterochromatin
n = 88

Figure S3: New H2A.X deposition in mouse embryonic fibroblasts. Related to Figures 1 and 2.
(A-C) Characterization by immunofluorescence (A), flow cytometry (B) and western-blot (C) of mouse NIH/3T3 cells stably expressing SNAP-tagged H2A.X and a GFP-tagged form of the UV damage sensor protein DDB2 (DNA Damage Binding protein 2, human sequence), which is defective in murine cells. GFP-DDB2 is then used to mark sites of UV damage repair. The percentage indicates H2A.X-SNAP levels relative to its endogenous form. (-: parental cell line; e: epitope tag)
(D) New H2A.X accumulation at sites of UVC damage marked by GFP-DDB2 analyzed 2 h after irradiation in NIH/3T3 cells stably expressing SNAP-tagged H2A.X and GFP-DDB2 and treated with Flavopiridol (+FLV).
(E) Low transcription levels in pericentric heterochromatin domains (DAPI-dense regions) revealed by Ethynyl-Uridine (EU)-mediated labeling of nascent transcripts in NIH/3T3 cells stably expressing H2A.X-SNAP and GFP-DDB2. Fluorescence profiles along the dotted line are displayed on the graph. a.u.: arbitrary units.
(F) New H2A.X accumulation in replicating pericentric heterochromatin (mid/late S-phase) analyzed in the absence of transcription inhibitor in NIH/3T3 cells stably expressing H2A.X-SNAP and GFP-DDB2. Ethynyl-deoxyUridine (EdU) labels replication foci.
Percentages of cells accumulating new H2A.X at UV sites or in replicating heterochromatin are shown on the graphs. Error bars represent SD from two independent experiments. A total of n cells were scored. Confocal images are shown in panels D-F. Scale bars, 10 μm.

Figure S4

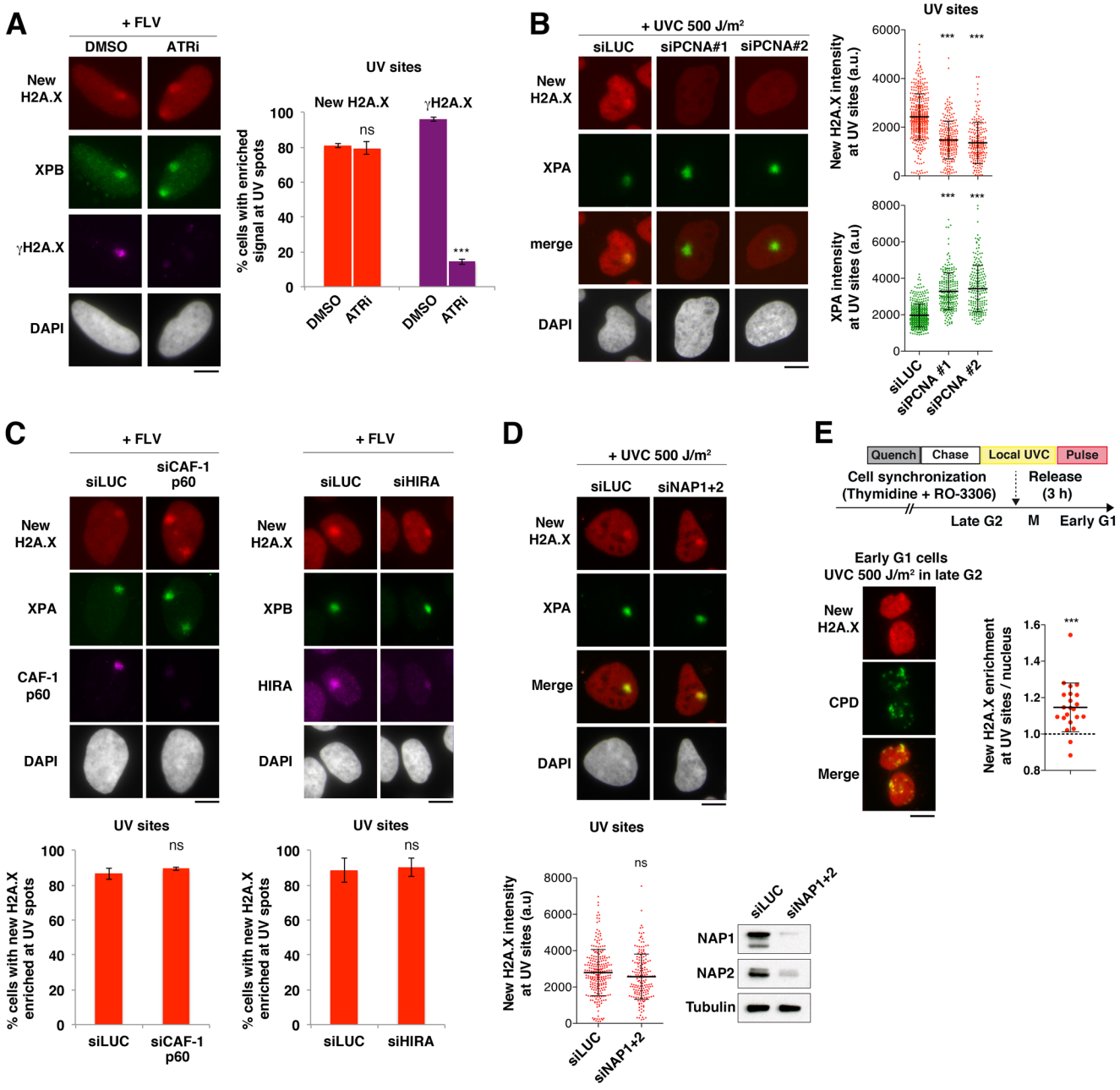
A
+ FLV
DMSO
ATRi
New H2A.X
XPB
γH2A.X
DAPI
UV sites
New H2A.X
γH2A.X
ns
***
% cells with enriched signal at UV spots
DMSO
ATRi
B
+ UVC 500 J/m²
siLUC
siPCNA#1
siPCNA#2
New H2A.X
XPA
merge
DAPI
UV sites
New H2A.X intensity at UV sites (a.u.)
XPA intensity at UV sites (a.u)
C
+ FLV
siLUC
siCAF-1 p60
siHIRA
XPB
HIRA
CAF-1 p60
% cells with new H2A.X enriched at UV spots
D
+ UVC 500 J/m²
siNAP1+2
Merge
New H2A.X intensity at UV sites (a.u)
NAP1
NAP2
Tubulin
E
Quench
Chase
Local UVC
Pulse
Cell synchronization (Thymidine + RO-3306)
Release (3 h)
Late G2
M
Early G1
Early G1 cells
UVC 500 J/m² in late G2
CPD
New H2A.X enrichment at UV sites / nucleus

Figure S4: Mechanistic insights into new H2A.X deposition at repair sites. Related to Figures 1, 3 and 4.
(A) New H2A.X accumulation at sites of UVC damage (marked by the repair factor XPB) is unaffected upon cell treatment with an ATR kinase inhibitor (ATRi; DMSO: vehicle) while H2A.X phosphorylation at UV sites (γH2A.X, purple) is severely reduced.
(B) New H2A.X accumulation 1h30 after local UVC irradiation in U2OS H2A.X-SNAP cells treated with the indicated siRNAs (siLUC: control). The intensity of new H2A.X signal (TMR fluorescence, red) and of the repair factor XPA (green) at UV sites are shown on the scatter plots (bars: mean; error bars: SD from at least 200 UV spots). Similar results were obtained in three independent experiments and data from one representative experiment are shown.
(C) New H2A.X accumulation at sites of UVC damage marked by XPA analyzed 2 h after irradiation in the presence of flavopiridol (+FLV) in U2OS cells stably expressing SNAP-tagged H2A.X and treated with the indicated siRNAs (siLUC: control). Knock-down efficiencies are verified by immunofluorescence (shown in purple) and western-blot (not shown). Percentages of cells accumulating new H2A.X at UV sites are shown on the graphs.
(**D**) New H2A.X accumulation 1h30 after local UVC irradiation in U2OS H2A.X-SNAP cells treated with the indicated siRNAs (siLUC: control). The intensity of new H2A.X signal at UV sites is shown on the scatter plot (bars: mean; error bars: SD from at least 180 UV spots). Similar results were obtained in two independent experiments and data from one representative experiment are shown. Knock-down efficiencies are verified by western-blot.
(**E**) Experimental scheme for irradiating cells synchronized in late G2 combined with the labeling of newly synthesized histones (Quench-Chase-Pulse). Cells were fixed in early G1 as shown on the immunofluorescence pictures (note that UV damage spots are scattered upon passage through mitosis). The enrichment of new H2A.X at UV sites (CPD) is shown on the scatter plot (bar: mean; error bars: SD from 22 cells). The significance of new H2A.X enrichment at UV sites is indicated (compared to a theoretical mean of 1, dotted line).
Error bars on the bar charts represent SD from two independent experiments. Scale bars, 10 μm.

Figure S5

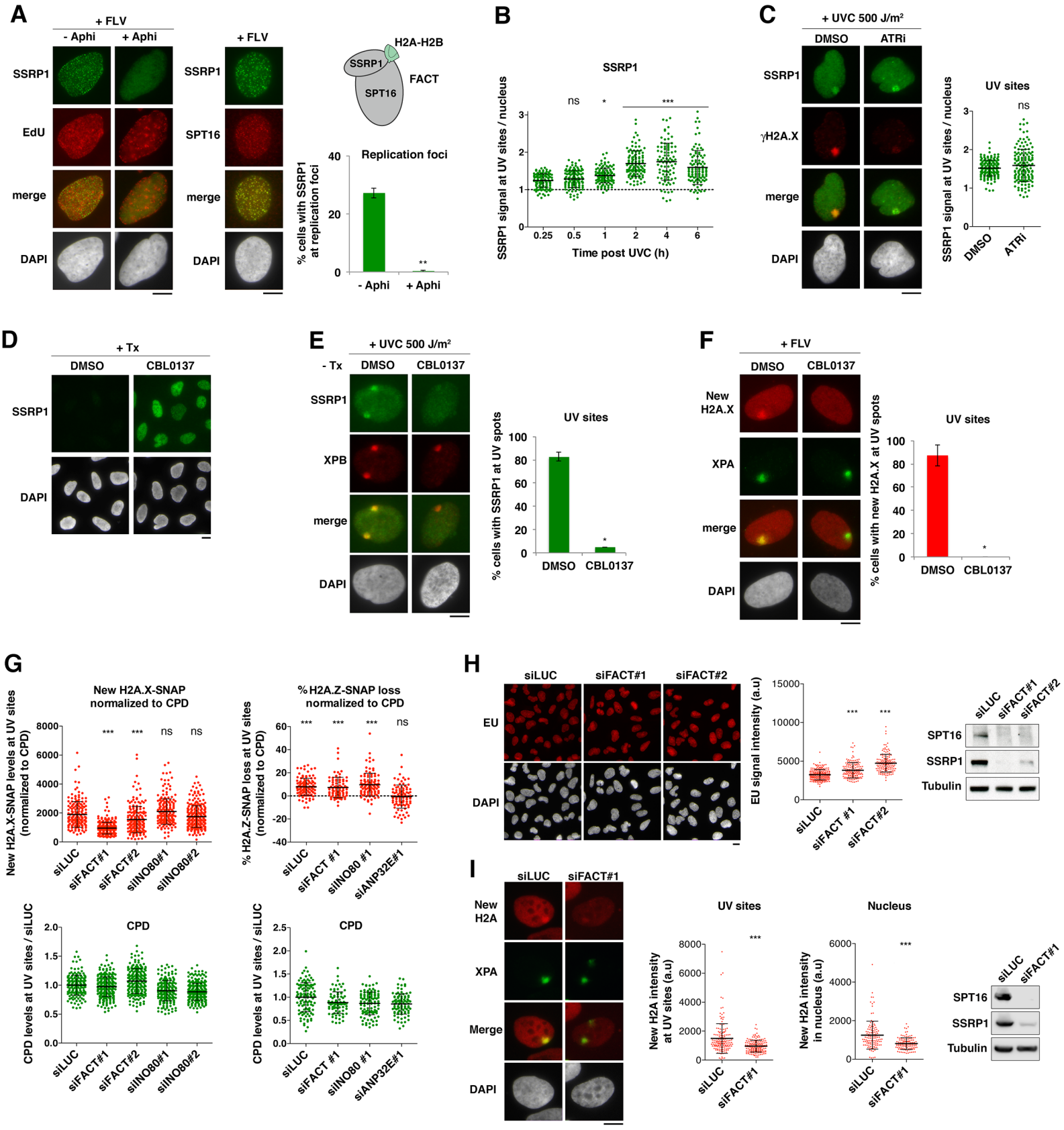
A
+ FLV
- Aphi
+ Aphi
SSRP1
EdU
merge
DAPI
SPT16
H2A-H2B
FACT
Replication foci
% cells with SSRP1 at replication foci
B
SSRP1
SSRP1 signal at UV sites / nucleus
Time post UVC (h)
C
+ UVC 500 J/m²
DMSO
ATRi
γH2A.X
UV sites
D
+ Tx
CBL0137
E
- Tx
XPB
% cells with SSRP1 at UV spots
F
New H2A.X
XPA
% cells with new H2A.X at UV spots
G
New H2A.X-SNAP levels at UV sites (normalized to CPD)
% H2A.Z-SNAP loss normalized to CPD
% H2A.Z-SNAP loss at UV sites (normalized to CPD)
siLUC
siFACT#1
siFACT#2
siINO80#1
siINO80#2
siANP32E#1
CPD
CPD levels at UV sites / siLUC
H
EU
EU signal intensity (a.u)
SPT16
SSRP1
Tubulin
I
New H2A
Merge
New H2A intensity at UV sites (a.u)
New H2A intensity in nucleus (a.u)
Nucleus

Figure S5: Role of FACT in H2A variant deposition. Related to Figures 4 and 5.
(A) *Left*, Recruitment of the FACT subunit SSRP1 to replication foci marked by EdU in U2OS cells treated with flavopiridol (+FLV). S-phase cells are labeled with EdU before Aphidicolin addition (+Aphi). Percentages of cells recruiting FACT to replication foci are shown on the graph. *Right*, Recruitment of both FACT subunits, SSRP1 and SPT16, to replication foci.
(**B**) Kinetics of FACT accumulation (SSRP1 subunit) at UV sites relative to the nucleus analyzed at the indicated time points post 500 J/m^2 local UVC irradiation in U2OS cells (bars: mean; error bars: SD from at least 89 UV spots). UV sites were marked with XPB and EdU to facilitate the detection of repair sites at late time points. Similar results were obtained in two independent experiments.
(**C**) Recruitment of the histone chaperone FACT (SSRP1 subunit) to UVC damage sites 2 h after local UVC irradiation at 500 J/m^2 in U2OS cells is not impaired by ATR inhibitor treatment (ATRi; DMSO, vehicle). Reduction of γH2A.X levels at UV sites shows the efficiency of ATR inhibition. SSRP1 enrichment at UV sites (delineated by XPB co-staining in a parallel experiment, not shown) is presented on the scatter plot (bars: mean; error bars: SD from at least 145 UV spots). Similar results were obtained in three independent experiments and data from one representative experiment are shown.
(D) Trapping of the histone chaperone FACT (SSRP1 subunit) on chromatin in U2OS cells treated with the intercalating agent curaxin (CBL0137; DMSO: vehicle). Detergent extraction of cells (+Tx) solubilizes FACT when not chromatin-bound.
(E) Impaired recruitment of the histone chaperone FACT (SSRP1 subunit) to repair sites marked by XPB 2 h after local UVC irradiation at 500 J/m^2 in U2OS cells treated with curaxin (CBL0137; DMSO: vehicle). Percentages of cells recruiting FACT to repair sites are shown on the graph.
(F) New H2A.X accumulation at sites of UVC damage marked by XPA analyzed 2 h after irradiation in the presence of flavopiridol (+FLV) in U2OS cells stably expressing SNAP-tagged H2A.X and treated with curaxin (CBL0137; DMSO: vehicle). Percentages of cells accumulating new H2A.X at repair sites are shown on the graph.
(**G**) New H2A.X levels and total H2A.Z loss at UVC damage sites analyzed as in Figure 4D and 5B, except that data were normalized to UV damage levels based on CPD counterstaining and H2A.Z data is presented as %loss at UV sites relative to the nucleus (bar: mean; error bars: SD from at least 84 UV spots). The significance of H2A.Z loss at UV sites is indicated (compared to a theoretical mean of 0%, dotted line). Similar results were obtained in two and three independent experiments, respectively, and data from one representative experiment are shown.
(H) Nascent transcription monitored by ethynyl-uridine (EU) incorporation in U2OS H2A.X-SNAP cells treated with the indicated siRNAs (siLUC: control; siFACT: combination of siSPT16 and siSSRP1). The efficiency of FACT knock-down is controlled by western-blot. Quantitation of EU levels in nuclei is shown on the scatter plot (bars: mean; error bars: SD from at least 140 cells). Similar results were obtained in three independent experiments and data from one representative experiment are shown.
(I) New H2A accumulation 1h30 after local UVC irradiation in U2OS H2A-SNAP cells treated with the indicated siRNAs (siLUC: control; siFACT: combination of siSPT16 and siSSRP1). Knock-down efficiencies are verified by western-blot. The intensity of new H2A signal (TMR fluorescence) at UV sites and in entire nuclei are shown on the graphs (bars: mean; error bars: SD from at least 150 cells). Similar results were obtained in four independent experiments and data from one representative experiment are shown.
Error bars on the bar charts represent SD from two independent experiments. Scale bars, 10 μm.

Figure S6

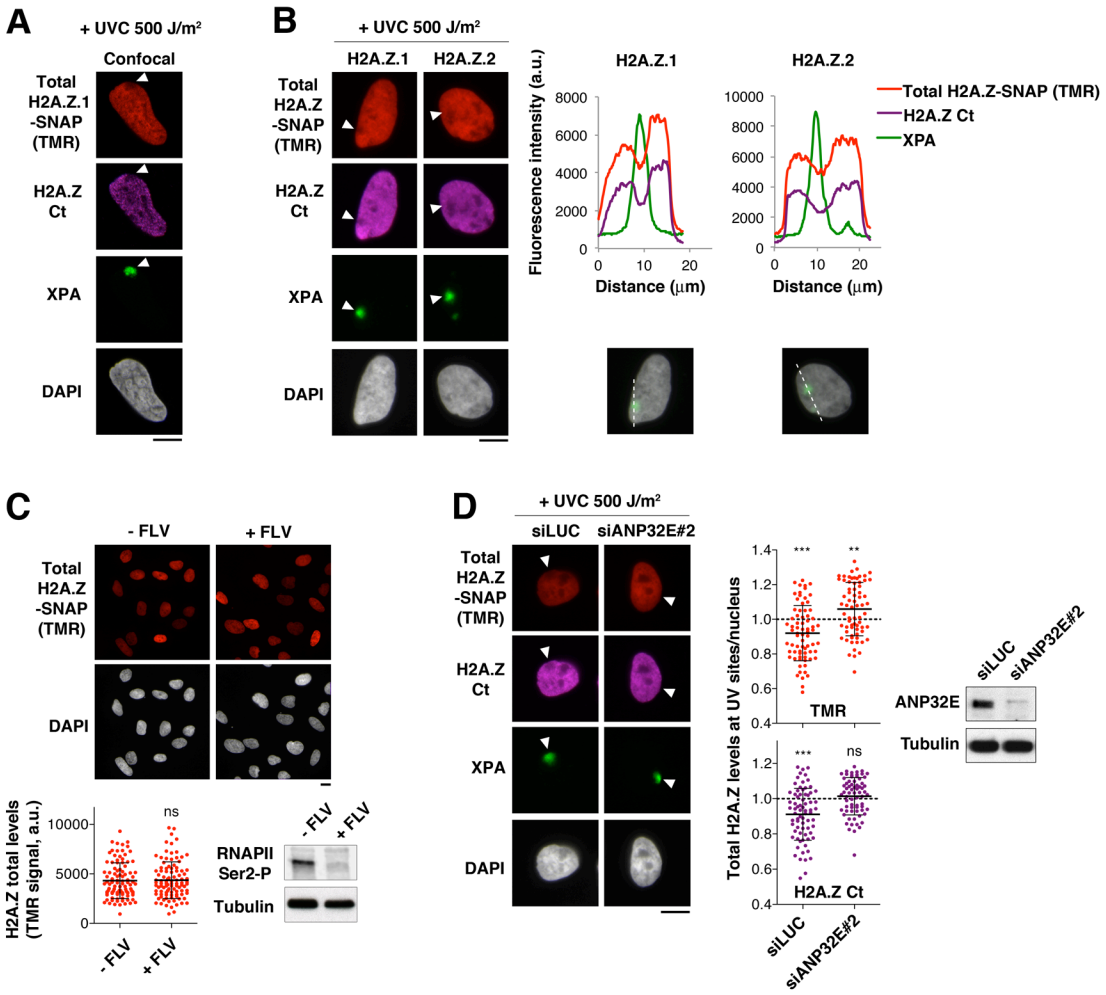
A
+ UVC 500 J/m²
Confocal
Total H2A.Z.1 -SNAP (TMR)
H2A.Z Ct
XPA
DAPI
B
+ UVC 500 J/m²
H2A.Z.1
H2A.Z.2
Total H2A.Z -SNAP (TMR)
H2A.Z Ct
XPA
DAPI
Fluorescence intensity (a.u.)
Distance (μm)
Total H2A.Z-SNAP (TMR)
H2A.Z Ct
XPA
C
- FLV
+ FLV
Total H2A.Z -SNAP (TMR)
DAPI
H2A.Z total levels (TMR signal, a.u.)
ns
RNAPII Ser2-P
Tubulin
D
+ UVC 500 J/m²
siLUC
siANP32E#2
Total H2A.Z -SNAP (TMR)
H2A.Z Ct
XPA
DAPI
Total H2A.Z levels at UV sites/nucleus
TMR
H2A.Z Ct
ANP32E
Tubulin

Figure S6: ANP32E-mediated depletion of H2A.Z at UV damage sites. Related to Figure 5.
(A, B) Distribution of total H2A.Z.1 and H2A.Z.2 1 h after local UVC irradiation (500 J/m^2) in U2OS cells expressing the indicated SNAP-tagged histone variants (A, confocal; B, epifluorescence images). Total levels of SNAP-tagged histones are detected by a pulse with SNAP-Cell TMR-star (TMR) before cell fixation and total H2A.Z is also revealed by immunostaining with an H2A.Z-specific antibody recognizing H2A.Z carboxy-terminus (Ct). The arrowheads point to sites of UV irradiation. Fluorescence intensity profiles along the dotted lines are shown on the graphs.
(C) Total H2A.Z levels detected by a pulse with SNAP-Cell TMR star before cell fixation in U2OS H2A.Z.1-SNAP cells treated or not with the transcription inhibitor flavopiridol (FLV) for 2 h. Transcription inhibition is verified by western-blot for the elongating from of RNAPII (Ser2-P). The intensity of total H2A.Z signal (TMR fluorescence) in nuclei is shown on the scatter plot (bar: mean; error bars: SD from at least 100 cells). Similar results were obtained in two independent experiments and also by staining total H2A.Z with specific antibodies (data not shown).
(D) Distribution of total H2A.Z analyzed 1 h after local UVC irradiation (500 J/m^2) in U2OS H2A.Z.1-SNAP cells treated with the indicated siRNAs (siLUC, control). Total levels of SNAP-tagged H2A.Z are detected by a pulse with SNAP-Cell TMR-star (TMR) before cell fixation and total H2A.Z is revealed by immunostaining with an H2A.Z-specific antibody recognizing H2A.Z carboxy-terminus (Ct). The arrowheads point to sites of UV irradiation. H2A.Z levels at UV damage sites relative to the whole nucleus are shown on the graphs (bars: mean; error bars: SD from at least 60 cells). The significance of H2A.Z loss or enrichment at UV sites is indicated (compared to a theoretical mean of 1, dotted line). Similar results were obtained in two independent experiments. ANP32E knock-down efficiency is shown on the western-blot panel. Scale bars, 10 μm.

Figure S7

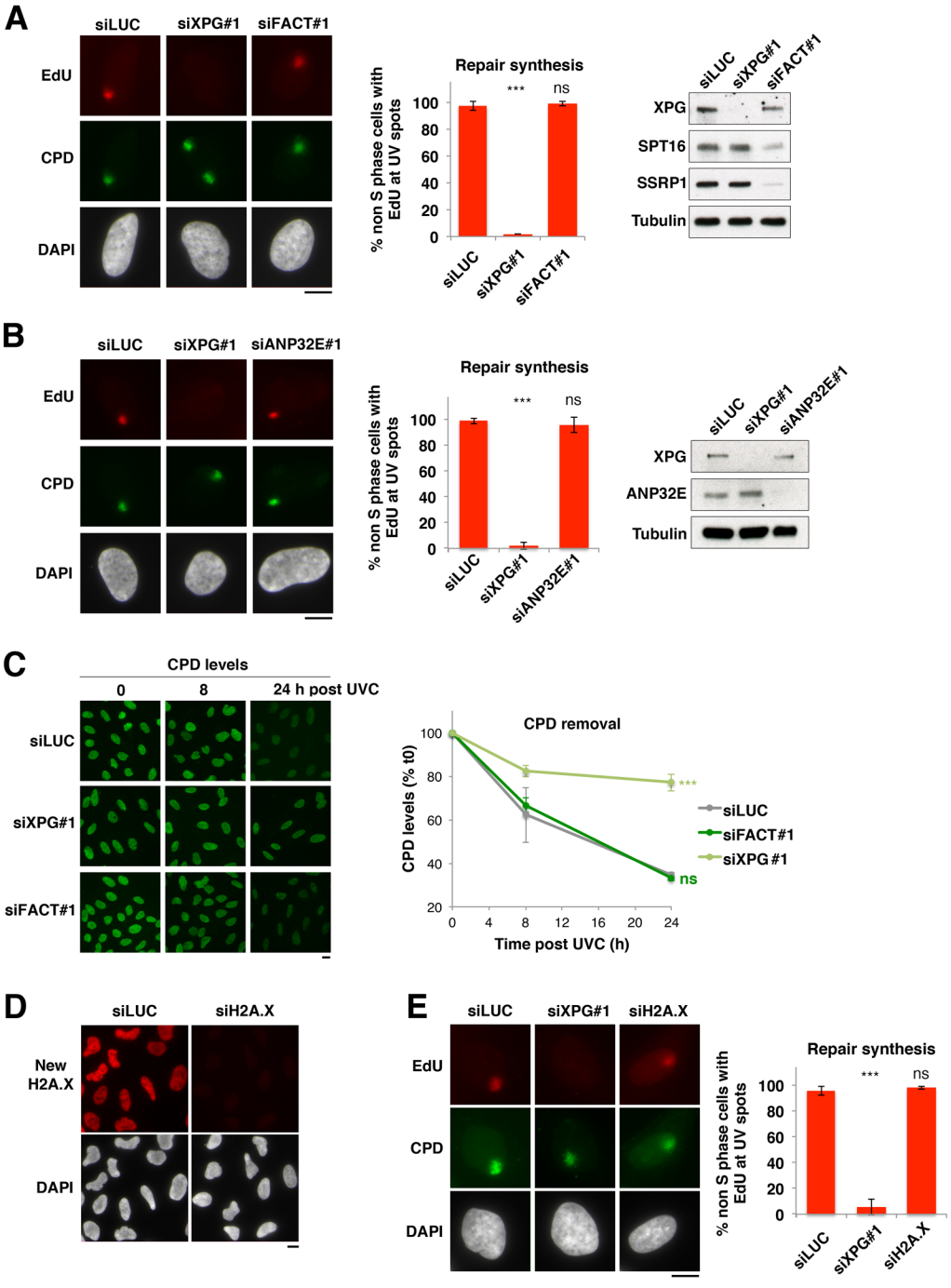
A
siLUC
siXPG#1
siFACT#1
EdU
CPD
DAPI
Repair synthesis
% non S phase cells with EdU at UV spots
***
ns
XPG
SPT16
SSRP1
Tubulin
B
siANP32E#1
ANP32E
C
CPD levels
0
8
24 h post UVC
CPD removal
CPD levels (% t0)
Time post UVC (h)
D
siH2A.X
New H2A.X
E

Figure S7: Role of FACT and ANP32E in UVC damage repair. Related to Figure 6.
(A, B, E) Repair synthesis at UV damage sites (CPD: Cyclobutane Pyrimidine Dimers) measured by EdU incorporation in U2OS cells treated with the indicated siRNAs (siLUC: control; siFACT: siSPT16+siSSRP1). siXPG is used as a positive control. Percentages of cells incorporating EdU at UV damage sites are shown on the graphs (mean ± SD from two independent experiments). Knockdown efficiencies are verified by western-blot.
(C) Kinetics of UV damage removal: immunostaining for UV photoproducts (CPD) at the indicated time points post global UVC irradiation in U2OS cells treated with the indicated siRNAs (siLUC: control; siFACT: siSPT16+siSSRP1). XPG siRNA is used as a positive control. Error bars, SEM from two independent experiments.
(D) H2A.X neosynthesis analyzed in U2OS cells stably expressing H2A.X-SNAP and treated with the indicated siRNAs (siLUC: control).
Scale bars, 10 μm.